Optics Communications 284 (2011) 5871–5876

Contents lists available at ScienceDirect

Optics Communications

journal homepage: www.elsevier.com/locate/optcom

Source sparsity based primal-dual interior-point method for three-dimensional bioluminescence tomography

Qitan Zhang [a], Heng Zhao [a], Duofang Chen [a], Xiaochao Qu [a], Xueli Chen [a], Xiaowei He [a], Wei Li [a], Zhenhua Hu [a], Junting Liu [a], Jimin Liang [a,*], Jie Tian [a,b,**]

[a] Life Sciences Research Center, School of Life Sciences and Technology, Xidian University, Xi'an 710071, China
[b] Institute of Automation, Chinese Academy of Sciences, Beijing 100190, China

ARTICLE INFO

Article history:
Received 16 December 2010
Received in revised form 3 March 2011
Accepted 28 July 2011
Available online 16 August 2011

Keywords:
Bioluminescence tomography
Inverse problem
Primal-dual interior-point method

ABSTRACT

In this paper, an efficient l_1-regularized reconstruction method named the primal-dual interior-point (PDIP) method is presented for three-dimensional bioluminescence tomography (BLT) based on the adaptive finite element framework. Taking into account the sparse characteristic of the bioluminescent source, the BLT inverse problem is considered to be a linear programming problem and is represented by its primal and dual form. The source localization and quantification are obtained by solving the primal-dual Newton equation system. The comparisons between PDIP and the classical conjugate gradient least square (CGLS) algorithm are implemented to validate our method. Results from numerical simulation and an *in vivo* mouse experiment demonstrate the credibility and the potential of the proposed method in practical BLT reconstruction.

1. Introduction

As a promising optical molecular imaging technique, bioluminescence tomography (BLT) suggests enormous potential in drug development and preclinical oncological investigation due to its significant advantages in specificity, sensitivity, safety and cost-effectiveness [1–4]. By integrating surface measured light flux distribution, geometrical structures and tissue optical properties, the goal of BLT is to reconstruct the distribution of bioluminescent probes inside a small living animal, achieving accurate tomographic reconstruction and visualization in three-dimensional (3D) [5–7]. However, the reconstruction problem remains a challenging issue because of the inherent ill-posedness nature of the inverse problem.

Recently, intensive interests have been given to the reconstruction algorithms and many feasible approaches have been proposed to handle the inverse source problem [6–18]. To alleviate the ill-posedness, some forms of *a priori* information have been employed to remarkably improve the source reconstruction, including permissible source region strategy that restricts the source in a specific area [8] and a spectrally-resolved approach that attains the reconstruction using multispectral data [9,17]. No matter what kind of *a priori* information used, the source reconstruction problem is regularized to a least squares optimization problem. Many numerical methods have been applied to solve this optimization problem, such as the conjugate gradient [13], level set strategy [7,14], trust region method [15] and a differential evolution approach [6]. Most of these methods are based on the l_2 norm regularization, which tries to solve the problem by combining a quadratic error term and an l_2 norm term. However, l_2 norm regularization has been proven to smooth solutions and bring multi-pseudo sources to surround the true source. Because of the sparsity of bioluminescent source distribution [16], l_1 regularization has been applied in BLT and became a mainstream trend [17,18].

In this paper, considering the sparse characteristic of the bioluminescent source, a primal-dual interior-point (PDIP) method was proposed for BLT reconstruction, which successfully integrates the adaptive finite element (AFE) framework and the l_1 norm regularization strategy. During the last twenty years, interior-point methods have been proven to be highly efficient in both theory and practice, which are robust for numerically solving optimization problems, such as linear, quadratic, second-order cone, geometric, and semidefinite programming [19–24]. The interior-point method was first proposed for solving linear programming problems by Karmarkar in 1984 [25]. By the early 1990s, a subclass of the interior-point methods distinguished itself as the most efficient practical approach, and turned out to be a strong competitor for large-scale problems. As the first approaches developed for solving sparse problems via convex optimization, interior-point methods have been widely applied in sparse signal reconstruction and processing, statistics, and related fields over the past few years [26]. As one branch of the interior-point methods, PDIP inherits the highly efficient and numerical robustness of the interior-point methods and it poses good convergence since it only requires a total of $O(\sqrt{n})$ iterations. As one of the best and

* Corresponding author. Tel./fax: +86 29 81891060.
** Correspondence to: J. Tian, Life Sciences Research Center, School of Life Sciences and Technology, Xidian University, Xi'an 710071, China. Tel.: +86 10 82618465; fax: +86 10 62527995.
E-mail addresses: jimleung@mail.xidian.edu.cn (J. Liang), tian@ieee.org (J. Tian).

0030-4018/$ – see front matter © 2011 Elsevier B.V. All rights reserved.
doi:10.1016/j.optcom.2011.07.071

most perfect polynomial algorithms of linear programming in theory, the PDIP combines the penalty function method and Newton method and can be used to resolve the sparse problem with l_1 regularization. Therefore, the PDIP method can be utilized to solve the source reconstruction problem in BLT.

In the proposed PDIP method, diffusion approximation (DA) was employed to describe light propagation in biological tissues. Based on the AFE framework, the DA is formalized as a linear matrix equation between the unknown source variables and the surface measurement. Because of the sparsity of the bioluminescent source distribution and the insufficiency of the surface measurement, the exact solution of the inverse source problem is the l_0 regularizer, which is one of the hardest combinatory optimization problems. In order to solve such a complicated problem, we replaced the l_0 regularizer with the l_1 norm for simplicity. By introducing the logarithmic barrier term, the PDIP method takes the l_1 norm problem as a minimization problem of linear programming. In order to obtain the optimal solution of the minimization problem, the Karush–Kuhn–Tucker (KKT) conditions were used to restrain the solving process. Using the Newton method, we obtained the optimal solution to the primal-dual equation. Reconstructed results on numerical simulation and an *in vivo* mouse experiment validated the ability of the proposed method for locating and quantifying the bioluminescent source.

2. Method

2.1. Forward formula of BLT

It is well acknowledged that the radiative transfer equation (RTE) can be used as the most accurate model to describe the photon transport in biological tissues [10,27]. However, due to the implementation complexity in a numerical setting and the difficulty in the direct calculation, the application of RTE for BLT is difficult [28]. Because photon transport in biological tissues exhibits high scattering and weak absorption, DA and its Robin boundary condition have been well accepted [8]:

$$\begin{array}{l} -\nabla\cdot(D(r)\nabla\Phi(r)) + \mu_a(r)\Phi(r) = S(r) \ \ (r\in\Omega) \\ \Phi(r) + 2A_n(r)D(r)(v(r)\cdot\nabla\Phi(r)) = 0 \ \ (r\in\partial\Omega) \end{array} \tag{1}$$

where $\Omega\subset R^3$ is the domain of interest ;$\mathbf{r}$ is a position vector; $\Phi(\mathbf{r})$ is the photon flux density; $S(\mathbf{r})$ is the source distribution; $\mu_a(\mathbf{r})$ is the absorption coefficient; $D(\mathbf{r})=1/(3(\mu_a(\mathbf{r})+\mu'_s(\mathbf{r}))$ is the diffusion coefficient, where $\mu'_s(\mathbf{r})$ is the reduced scattering coefficient; $v(\mathbf{r})$ is the unit outer normal on the boundary $\partial\Omega$; and $A_n(\mathbf{r})=(1+R(\mathbf{r}))/(1-R(\mathbf{r}))$ is the boundary mismatch factor, where $R(\mathbf{r})$ depends on the refractive index n of the surrounding medium and can be approximated by $R\approx -1.4399n^{-2}+0.7099n^{-1}+0.6681+0.0636n$ [29]. In the bioluminescence imaging experiments, the exiting flux density on $\partial\Omega$ can be can be expressed as follows [8]:

$$Q(\mathbf{r}) = -D(r)(v(r)\cdot\nabla\Phi(r)) = -\frac{1}{2A_n(r)}\Phi(r)\ (r\in\partial\Omega). \tag{2}$$

Using the AFE framework [30] and taking into account *a priori* knowledge of the permissible source region, a simple linear relationship between the measurable boundary data and the unknown source distribution is established:

$$AS^p = \Phi^m \tag{3}$$

where $\mathbf{A}$ is the system matrix and is formed by removing the rows associated with immeasurable photon fluence rate on interior nodes, $\mathbf{S}^p$ is the source density in the permissible source region, and Φ^m is the measurable photon fluence rate on boundary nodes.

2.2. Primal-dual interior-point method for BLT reconstruction

Because of the insufficient measurement and the ill-conditioned system matrix, Eq. (3) is underdetermined and ill-posed. To deal with the ill-posedness, the BLT reconstruction is regularized as the following regularization problem [16]:

$$\begin{cases} min\,||S^p||_0 \\ s.t.\ AS^p = \Phi^m \\ \quad S^p\geq 0 \end{cases} \tag{4}$$

where $||\cdot||_0$ denotes the l_0 norm. Because of the combinatorial difficulty and the exponential complexity, l_0 norm is usually equivalent to the l_1 norm regularization problem based on the compressive sensing theory [16]:

$$\begin{cases} min\,||S^p||_1 \\ s.t.\ AS^p = \Phi^m . \\ \quad S^p\geq 0 \end{cases} \tag{5}$$

In order to solve the l_1 norm problem, the linear programming problem (5) should be translated into the following standard form, the primal and its dual form [20,22,31]:

$$\begin{cases} P:\ minc^T x \\ s.t.\ Ax = b \\ \quad x\geq 0 \end{cases} \quad \begin{cases} D:\ max\, b^T y \\ s.t. A^T y + s = c \\ \quad s\geq 0 \end{cases} \tag{6}$$

where $\mathbf{c}$, $\mathbf{s}$ and $\mathbf{x}$ are vectors in R^n, $\mathbf{b}$ and $\mathbf{y}$ are vectors in R^m, and $\mathbf{A}$ is an $m\times n$ matrix. Here $\mathbf{x}$ and $b$stand for $\mathbf{S}^p$ and Φ^m respectively. Given a feasible solution $\mathbf{x}$ of P and a feasible solution $(\mathbf{y},\mathbf{s})$ of D, the duality gap is simply obtained as:

$$c^T x - b^T y = x^T s \geq 0. \tag{7}$$

Let us introduce a logarithmic barrier term for P. For barrier parameter $\theta>0$, we obtain:

$$\begin{cases} P(\theta):\ min\, c^T x - \theta\sum_{j=1}^{n} In\, x_j \\ s.t.\ Ax = b \\ \quad x\geq 0. \end{cases} \tag{8}$$

Because the gradient of the objective function $P(\theta)$ is $\mathbf{c}-\theta\mathbf{X}^{-1}\mathbf{e}$ (where $\mathbf{e}$ is the vector of ones), the KKT conditions for $P(\theta)$ are [20]:

$$\begin{cases} Ax = b, x\ N\ 0 \\ A^T y + s = c \\ XSe/\theta - e = 0 \end{cases} \tag{9}$$

where $\mathbf{X}$ is a $n\times n$ diagonal matrix whose diagonal entries are precisely the components of $\mathbf{x}$; $\mathbf{S}$ is the $n\times n$ diagonal matrix whose diagonal entries are precisely the components of $\mathbf{s}$, and $\mathbf{s}$ is defined by $\mathbf{s}=\theta\mathbf{X}^{-1}\mathbf{e}$.

From (9), we obtain that if $(\mathbf{x},\mathbf{y},\mathbf{s})$ is a solution of (9), then $\mathbf{x}$ is feasible for P, $(\mathbf{y},\mathbf{s})$is feasible for D, and the resulting duality gap is:

$$x^T s = e^T X\, S\, e = \theta\, n. \tag{10}$$

This suggests that we tried solving $P(\theta)$ for a variety of values of θ as $\theta\to 0$.

Assuming the next feasible point is $(\overline{x},\overline{y},\overline{s})$, we calculated the primal-dual Newton direction $(\Delta\mathbf{x},\Delta\mathbf{y},\Delta\mathbf{s})$ based on the Newton

method. Because $(\bar{x},\bar{y},\bar{s})$ satisfies (10), we obtain the following system equation:

$$\begin{cases} A\Delta x = b - Ax \\ A^T\Delta y = c - A^T y - s \\ S\Delta x + X\Delta s = \theta e - XSe \end{cases}. \tag{11}$$

By solving (11), we obtain the primal-dual Newton direction and a new feasible point.

Based on the above analysis, we are motivated to develop the primal-dual interior-point algorithm for BLT reconstruction. The general framework for the proposed algorithm is described as follows:

Step 1: Initialization. Given that $(\mathbf{x}^0,\mathbf{y}^0,\mathbf{s}^0,\theta)$ satisfies $\mathbf{x}^0>0, \mathbf{s}^0>0$, $\mathbf{y}^0$ is a random vector and $\theta>0$, step-factor h satisfies $0<h<1$ and the tolerance parameter $\varepsilon>0$. Set $k\leftarrow 0$.

Step 2: Check the following stopping criterions.

$$(1)\|Ax^k - b\| < \varepsilon$$
$$(2)\|A^T y^k + s^k - c\| < \varepsilon.$$
$$(3)\left(s^k\right)^T x^k < \varepsilon$$

If one of the above three conditions is met, then the reconstruction is stopped. If not, proceed.

Step 3: Shrink θ. Set $\theta\leftarrow\alpha\theta$ for decreasing the parameter $\alpha\in(0,1)$.

Step 4: Compute the primal-dual Newton direction. Compute the Newton direction $(\Delta\mathbf{x},\Delta\mathbf{y},\Delta\mathbf{s})$ using (11) at $(\mathbf{x}^k,\mathbf{y}^k,\mathbf{s}^k)$ for θ.

Step 5: Determine the step-sizes.

$$\theta_P = \min\left\{1, h\min_{\Delta x_j<0}\left\{\frac{x_j^k}{-\Delta x_j}\right\}\right\}, \theta_D = \min\left\{1, h\min_{\Delta s_j<0}\left\{\frac{s_j^k}{-\Delta s_j}\right\}\right\}.$$

Step 6: Update values.

$$\left(x^{k+1}, y^{k+1}, s^{k+1}\right)\leftarrow\left(x^k + \theta_P\Delta x, y^k + \theta_D\Delta y, s^{k+1} + \theta_D\Delta s\right).$$

Reset $k\leftarrow k+1$ and return to *Step 2*.

3. Experiments and results

In this section, a series of verification experiments were designed to evaluate our proposed reconstruction algorithm. In order to analyze the results quantitatively, we defined the Location Error of the distance between the actual and reconstructed source and the Relative Error of the source density between the actual and reconstructed source as follows:

$$\textit{Location Error} = \sqrt{(x-x_0)^2 + (y-y_0)^2 + (z-z_0)^2}$$
$$\textit{Relative Error} = |S_{recon} - S_{real}| / S_{real}$$

where (x,y,z) is the coordinate of the reconstructed source with the maximum density and (x_0,y_0,z_0) is that of the actual source center; S_{recon} and S_{real} are the density of the reconstructed source and the actual source respectively. All of the results were compared with the conjugate gradient least square (CGLS) algorithm, which is a classical method to solve the l_2 norm problem. In all experiments, we set the max iterations of the PDIP and CGLS to 10 and the initial values of $\mathbf{x}$ are manually optimized between the zero vector and the vector of ones; the initial values of $\mathbf{y}$ and $\mathbf{s}$ are the random vector; the barrier parameter $\theta=1$; the tolerance parameter $\varepsilon=1e-8$; the step-factor $h=0.99$; the decreasing parameter $\alpha=0.1$ and the regularization parameter of CGLS is $1e-9$. Both reconstruction algorithms were coded in MATLAB and carried out on a personal computer with 2.66 GHz Intel Core 2 Quad CPU and 4 GB RAM.

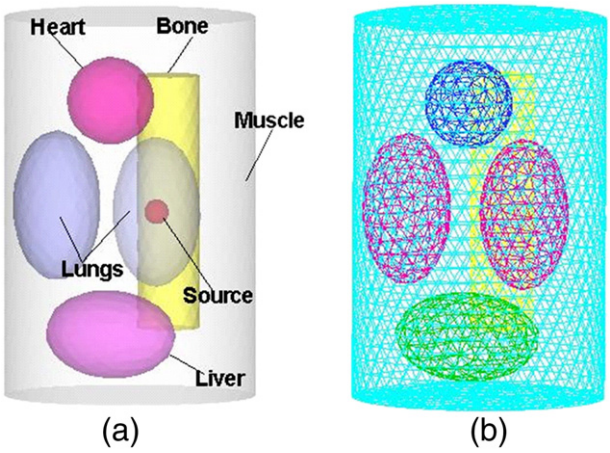

Fig. 1. Heterogeneous phantom. (a) A heterogeneous phantom with a single light source, consisting of muscle, lungs, heart, bone, liver and the source in the right lung; (b) The initial mesh used in the adaptive FEM algorithm.

3.1. Numerical experiment

We first considered two numerical cases to verify our proposed method. In this part, a cylindrical heterogeneous phantom was employed (30 mm height and 20 mm diameter). It contained five kinds of materials to represent muscle, lungs, heart, bone and liver respectively, as shown in Fig. 1(a) [11]. Optical parameters that came from the literature [30] were assigned to each of the five components, as listed in Table 1. Because the Monte Carlo (MC) method remains as the gold standard for photon transport simulation in biological tissues, the Molecular Optical Simulation Environment (MOSE), which was developed based on the MC method, was used to obtain the objective and reliable surface measured data in this section [32]. It was difficult to obtain all of the surface data from the cylindrical phantom in the imaging experiment, hence only the data on side of the cylinder were used for source reconstruction in this paper.

In single source case, the phantom was discretized into 3874 nodes and 17763 tetrahedral elements. A solid sphere source with a 1 mm radius and 0.238 nW/mm^3 power density was centered at (3, 5, 0) inside of the right lung as shown in Fig. 1(a). In the reconstruction procedure, a coarse volumetric mesh shown in Fig. 1(b) was chosen as the initial discretization of the phantom. Furthermore, in order to reduce the number of unknown variables, the entire right lung was specified as an *a priori* permissible source region.

After two steps of refining the procedure of the AFE framework, we obtained the BLT reconstruction results using PDIP and CGLS respectively, as shown in Fig. 2. The reconstructed location of our proposed algorithm was (2.864, 4.618, and −0.068) with a location error of 0.470 mm, and the reconstructed power density was 0.231 nW/mm^3 with a relative error of 2.93%. In contrast, the reconstructed location of the CGLS algorithm was (2.897, 7.025, and −0.214) with a location error of 2.039 mm, and the reconstructed power density was 0.127 nW/mm^3 with a relative error of 46.64%. It is shown that the method proposed in this paper provided a superior final result than the CGLS algorithm.

Table 1
Optical parameters of the heterogeneous phantom [30].

Tissue	μ_a (mm^{-1})	μ'_s (mm^{-1})
Muscle	0.010	0.400
Heart	0.200	2.400
Lungs	0.350	1.380
Liver	0.035	0.600
Bone	0.002	2.000

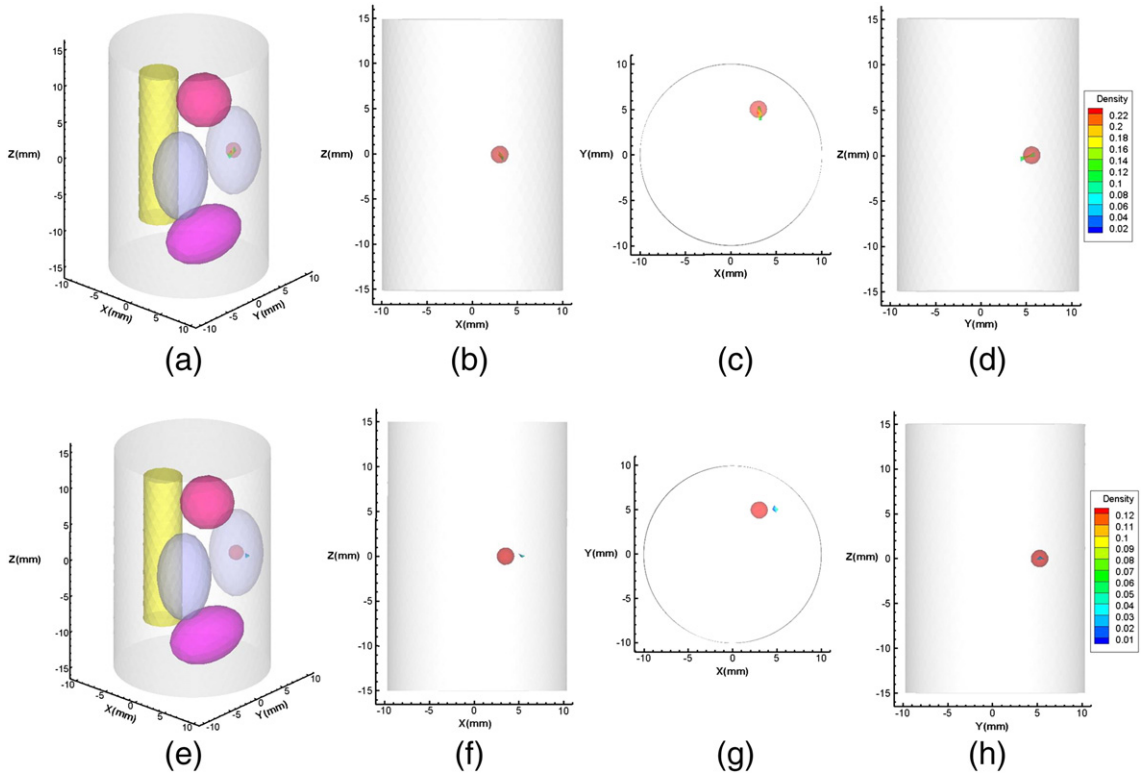

Fig. 2. Result comparisons between the actual and reconstructed sources using PDIP and CGLS in single source case. (a)–(d) are the reconstructed results by PDIP, (e)–(h) are the reconstructed results using CGLS; (a) and (e) are 3D views, (b) and (f) are coronal views, (c) and (g) are axial views, and (d) and (h) are sagittal views.

In the case of double source reconstruction, two solid sphere sources with a 1 mm radius and 0.238 nW/mm^3 power density were centered at (3, 5, 2) and (3, 5, −2) inside of the right lung as shown in Fig. 3(a). The right lung was still specified as an *a priori* permissible source region and the ultima mesh was 4002 nodes and 18,086 tetrahedral elements after two refined steps. The reconstruction

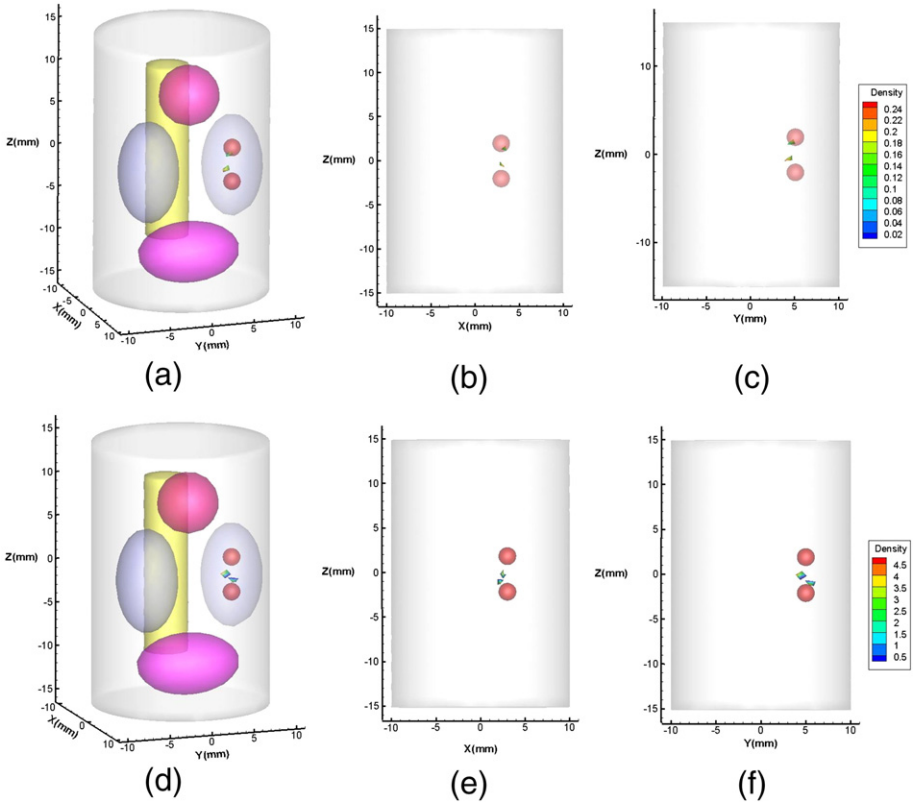

Fig. 3. Result comparisons between the actual and reconstructed sources using PDIP and CGLS in double source reconstruction. (a)–(c) are the reconstructed results by PDIP, (d)–(f) are the reconstructed results using CGLS; (a) and (d) are 3D views, (b) and (e) are coronal views, and (c) and (f) are sagittal views.

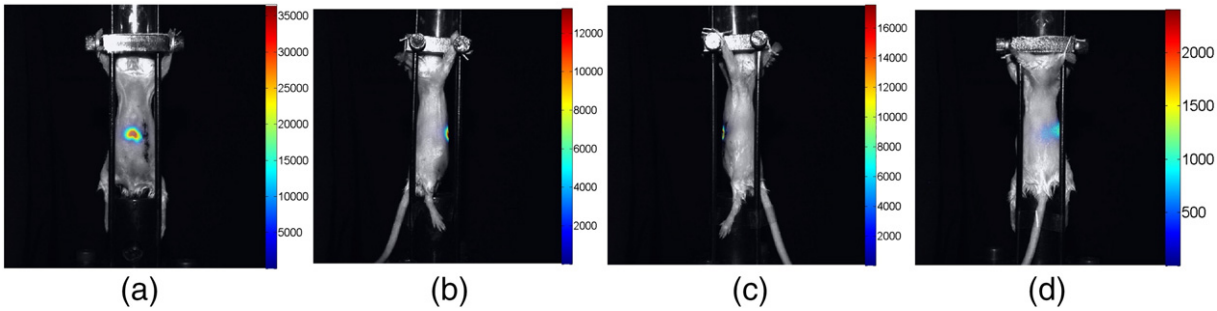

Fig. 4. Multi-view overlay images from photographs and photographic images (in pseudo color) of the mouse torso using a CCD camera in four directions, 90° apart. (a)–(d) Anterior–posterior, right lateral, left lateral, and posterior–anterior views respectively.

results using PDIP and CGLS are shown in Fig. 3. The reconstructed locations of PDIP were (3.528, 4.779, and 1.754) and (3.394, 3.800, and −0.702) with the location errors of 0.626 mm and 1.811 mm, and the reconstructed power densities were 0.225 nW/mm^3 and 0.252 nW/mm^3 with the relative errors of 5.46% and 5.88%. In contrast, the reconstructed locations of the CGLS were (2.500, 3.862, and 0.326) and (2.194, 5.396, and −1.158) with the location errors of 2.327 mm and 1.231 mm, and the reconstructed power densities were 4.429 nW/mm^3 and 4.477 nW/mm^3. In Fig. 3(a)–(c), we can see that the two sources can be accurately distinguished by PDIP, but the reconstructed sources of CGLS are close to each other in Fig. 3(d)–(f). The reconstructed results demonstrated that the PDIP method can bring good spatial resolution and satisfactory quantitative results.

3.2. In vivo experiment

An *in vivo* experiment was presented here to verify the performance of the proposed method for mouse applications. A catheter containing a luminescent liquid was implanted into a living mouse as the test source. The luminescent liquid was extracted from a luminescent mini Glowproducts stick (Glowproducts, Victoria, Canada) with an emission peak wavelength of about 644 nm, whose emission spectrum is similar to the *in vivo* spectrum of a firefly luciferase-based source. The light source was 2.7 mm in diameter and 5.1 mm in length, with an initial power density of 60 nW/mm^3. Two dimensional photographic images of the surface emitted photon flux were captured using a BLT prototype imaging system as shown in Fig. 4. The CCD camera in the experimental system was calibrated by an integrating sphere of 12 in. in diameter (USS-1200V-LL Low-Light Uniform Source, Labsphere, North Sutton, NH) [33]. Meanwhile, luminescent images performed the mapping to the object surface and processed them as normalized results [34].

The mouse torso section was scanned using micro-CT and segmented into major anatomical components, including muscle, heart, lungs, liver and kidneys. The optical parameters of each organ are listed in Table 2 [5]. In the mouse experiment, the coordinates (19.68, 18.40, and 19.20) of the actual source's center were obtained by micro-CT scanning. The permissible source region was set to be $P=\{(x,y,z)|0<x<100, 15<y<21, 10<z<30\}$ according to the surface photon flux distribution mapped from two-dimensional photographic images. The model was discretized into 6503 nodes and 32578 tetrahedral elements. The reconstruction results are shown in Fig. 5.

Table 2
Optical parameters of the organs of the mouse [5].

Organ	μ_a (mm^{-1})	μ'_s (mm^{-1})
Muscle	0.009	1.258
Heart	0.138	1.077
Lungs	0.460	2.265
Liver	0.829	0.736
Kidney	0.155	2.533

The reconstructed location of our proposed algorithm was (20.06, 18.85, and 18.95) with a location error of 0.64 mm, and the reconstructed power density was 56.638 nW/mm^3 with a relative error of 5.60%. The reconstructed location of the CGLS algorithm was (19.82, 14.29, and 19.33) with a location error of 4.11 mm, and the reconstructed power density was 2.61 nW/mm^3 with a relative error of 95.65%. As shown in Fig. 5(g) and (h), we see that the reconstructed source is near the edge of the mouse torso. In contrast, we obtained good results by utilizing the proposed method in Fig. 5(c) and (d). In the *in vivo* experiment, the PDIP achieved better reconstruction than the CGLS in localization and quantification of the luminescence source.

4. Conclusion and discussion

Because of the ill-posedness of the BLT inverse problem, multiple solutions and aberrant source reconstructions are frequent problems. Therefore, regularization methods are generally adopted to ease ill-posedness in the inverse problem. Among these methods, l_1 regularization has become a powerful tool for solving the underdetermined inverse problem because of the inherent sparse distribution characteristics of the bioluminescence source and the insufficient measurement data in BLT. In this paper, we presented an l_1-norm-based primal-dual interior-point method for the first time for the BLT inverse problem. In order to assess and analyze the reliability of the proposed method, we carried out two experiments.

In the numerical simulation, we used MC-based synthetic data to reconstruct the BLT source. Despite the location error or the relative error of the source density, PDIP yielded better results than that of CGLS in the single source simulation. Although the multiple source reconstruction was very challenging and unstable, the PDIP method still obtained encouraging results compared to the CGLS method in terms of spatial resolution and the quantitative results in double source simulation. In the *in vivo* mouse experiment where the source was in deeply embedded locations, PDIP still had more accurate and robust results than CGLS. The experimental reconstructions further showed the possibility of utilizing the PDIP method for complex *in vivo* mouse BLT applications. We can see that the results of CGLS are close to the edge of the permissible source region in Fig. 5. It is due to the fact that PDIP is based on l_1 regularization and the l_1 regularization method tends to provide better initial results and obtain more sparse solutions than the l_2 regularization method.

However, there is a limitation to the proposed method in that the run time of PDIP still needs to be improved with respect to CGLS. However, this problem could be solved if we consider continuation. The idea of continuation has been shown to be a very successful tool to improve the speed of convergence, especially when dealing with large-scale problems and highly dynamic range signals.

In conclusion, we developed a new reconstruction method for three-dimensional BLT and demonstrated its feasibility and accuracy in numerical simulation and an *in vivo* experiment. In future work, we

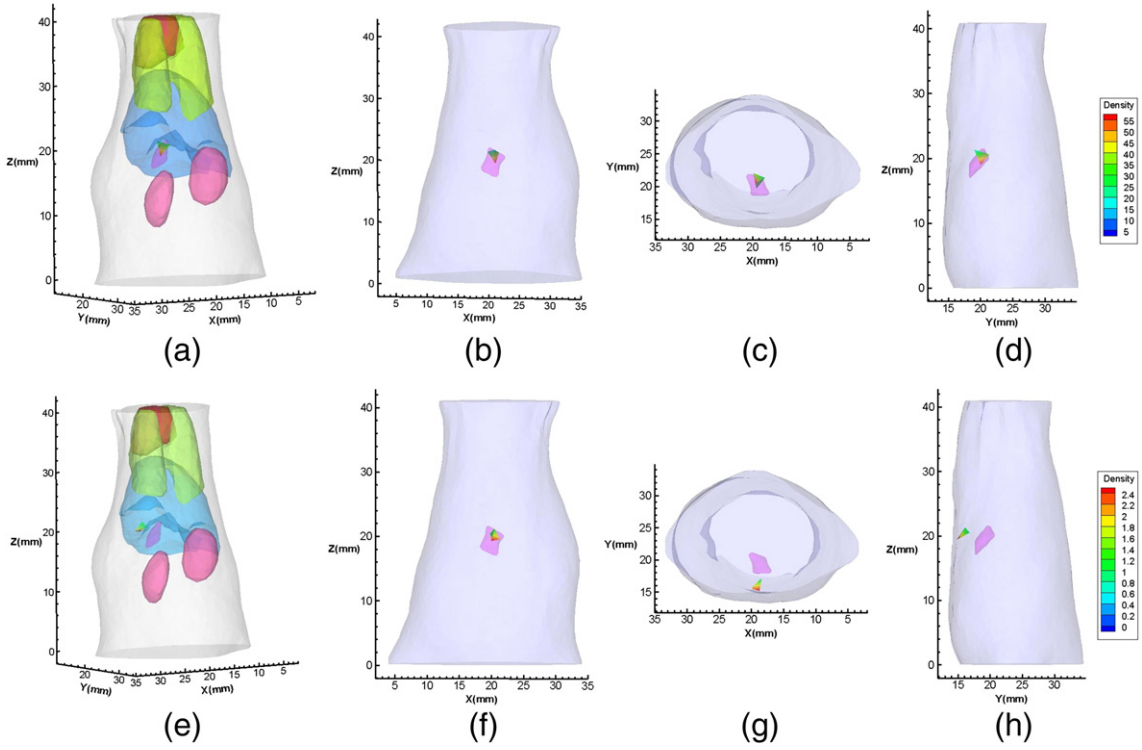

Fig. 5. Reconstructed results using PDIP and CGLS in the mouse experiment. (a)–(d) are the reconstructed results using PDIP, (e)–(h) are the reconstructed results using CGLS; (a) and (e) are 3D views, (b) and (f) are coronal views, (c) and (g) are axial views, and (d) and (h) are sagittal views.

will develop a new interior-point algorithm with the continuation technique to improve the primal-dual interior-point method. I*n vivo* mouse tumor studies will be reported in the future as well.

Acknowledgments

This work is supported by the Program of the National Basic Research and Development Program of China (973) under Grant Nos. 2011CB707702, the National Natural Science Foundation of China under Grant Nos. 81090272, 81000632, and 30900334, the Shaanxi Provincial Natural Science Foundation Research Project under Grant No. 2009JQ8018, and the Fundamental Research Funds for the Central Universities.

References

[1] C.H. Contag, B.D. Ross, J. Magn. Reson. Imaging 16 (2002) 378.
[2] R. Weissleder, M.J. Pittet, Nature 452 (2008) 580.
[3] G. Wang, E.A. Hoffman, G. McLennan, L.V. Wang, M. Suter, J.F. Meinel, Radiology 566 (2003) 229.
[4] G. Wang, Y. Li, M. Jiang, Med. Phys. 31 (2004) 2289.
[5] G. Alexandrakis, F.R. Rannou, A.F. Chatziioannou, Phys. Med. Biol. 50 (2005) 4225.
[6] A. Cong, W. Cong, Y. Lu, P. Santago, A. Chatziiouannou, G. Wang, IEEE Trans. Biomed. Eng. 57 (2010) 2229.
[7] K. Liu, X. Yang, D. Liu, C. Qin, J. Liu, Z. Chang, M. Xu, J. Tian, J. Opt. Soc. Am. A 27 (2010) 1413.
[8] W. Cong, G. Wang, D. Kumar, Y. Liu, M. Jiang, L.V. Wang, E.A. Hoffman, G. McLennan, P.B. McCray, J. Zabner, A. Cong, Opt. Express 13 (2005) 6756.
[9] H. Dehghani, S.C. Davis, S. Jiang, B.W. Pogue, K.D. Paulsen, M.S. Patterson, Opt. Lett. 31 (2006) 365.
[10] A.D. Klose, V. Ntziachristos, A.H. Hielscher, J. Comput. Phys. 202 (2005) 323.
[11] Y. Lv, J. Tian, W. Cong, G. Wang, J. Luo, W. Yang, H. Li, Opt. Express 14 (2006) 8211.
[12] X. Cheng, Rong. Gong, W. Han, J. Eng. Math. 63 (2009) 121.
[13] S. Ahn, A.J. Chaudhari, F. Darvas, C.A. Bouman, R.M. Leahy, Phys. Med. Biol. 53 (2008) 3921.
[14] H. Huang, X. Qu, J. Liang, X. He, X. Chen, D. Yang, J. Tian, J. Comput. Phys. 229 (2010) 5246.
[15] B. Zhang, X. Yang, C. Qin, D. Liu, S. Zhu, J. Feng, L. Sun, K. Liu, D. Han, X. Ma, X. Zhang, J. Zhong, X. Li, X. Yang, J. Tian, Opt. Express 18 (2010) 6477.
[16] W. Cong, G. Wang, J. Opt. Soc. Am. A 27 (2010) 174.
[17] Y. Lu, X. Zhang, A. Douraghy, D. Stout, J. Tian, T.F. Chan, A.F. Chatziioannou, Opt. Express 17 (2009) 8062.
[18] H. Gao, H. Zhao, Opt. Express 18 (2010) 2894.
[19] C. Mészáros, SIAM J. Matrix Anal. Appl. 30 (2008) 223.
[20] S. Wright, Primal-dual Interior-point Methods, Society for Industrial and Applied Mathematics, SIAM, Philadelphia, PA, 1997.
[21] Y. Ye, Interior Point Algorithms: Theory and Analysis, John Wiley and Sons, New York, 1997.
[22] Y. Nesterov, A. Nemirovsky, Interior-point Polynomial Methods in Convex Programming, SIAM, Philadelphia, PA, 1994.
[23] C. Johnson, J. Seidel, A. Sofer, IEEE Trans. Med. Imaging 19 (2000) 271.
[24] L. Portugal, M. Resende, G. Veiga, J. Júdice, Networks 35 (2000) 91.
[25] N. Karmarkar, Combinatorica 4 (1984) 373.
[26] S.J. Kim, K. Koh, M. Lustig, S. Boyd, D. Gorinevsky, IEEE J Sel Top Signal Process 1 (2007) 606.
[27] L.V. Wang, Hsin-i Wu, Biomedical Optics: Principles and Imaging, John Wiley and Sons, New York, 2007.
[28] M. Chu, K. Vishwanath, A.D. Klose, H. Dehghani, Phys. Med. Biol. 54 (2009) 2493.
[29] M. Schweiger, S. Arridge, M. Hiraoka, D. Delpy, Med. Phys. 22 (1995) 1779.
[30] R. Han, J. Liang, X. Qu, Y. Hou, N. Ren, J. Mao, J. Tian, Opt. Express 17 (2009) 14481.
[31] R.M. Freund, Primal-Dual Interior-Point Methods for Linear Programming Based on Newton's Method, Massachusetts Institute of Technology, 2004.
[32] N. Ren, J. Liang, X. Qu, J. Li, B. Lu, J. Tian, Opt. Express 18 (2010) 6811.
[33] J. Liu, Y. Wang, X. Qu, X. Li, X. Ma, R. Han, Z. Hu, X. Chen, D. Sun, R. Zhang, D. Chen, D. Chen, X. Chen, J. Liang, F. Cao, J. Tian, Opt. Express 18 (2010) 13102.
[34] X. Chen, X. Gao, D. Chen, X. Ma, X. Zhao, M. Shen, X. Li, X. Qu, J. Liang, J. Ripoll, J. Tian, Opt. Express 18 (2010) 19876.